Supporting Information

In situ spectroscopic investigations of MoO_x/Fe_2O_3 catalysts for the selective oxidation of methanol

Catherine Brookes,[a,b] Peter P. Wells,*[,a,c] Emma K. Gibson,[a,c] Diego Gianolio,[d] Khaled M. H. Mohammed,[a,c,e] Stephen Parry,[d] Scott M. Rogers,[a,c] Ian P. Silverwood,[a,c] and Michael Bowker*,[a,b]

a. UK Catalysis Hub, Research Complex at Harwell, Rutherford Appleton Laboratory, Harwell, Oxon, OX11 0FA

b. Cardiff Catalysis Institute, School of Chemistry, Cardiff University, Park Place, Cardiff, CF10 3AT, UK

c. Department of Chemistry, University College London, 20 Gordon St., London, WC1H 0AJ, UK

d. Diamond Light Source, Harwell Science and Innovation Campus, Didcot, Oxon, OX11 0DE, UK

e. Chemistry Department, Faculty of Science, Sohag University, Sohag, P.O.B 82524, Egypt.

Approximate weight percentage of Mo for 1 ML MoO_x/Fe_2O_3:

The approximate weight percent of molybdenum can be estimated as a useful comparison with the value obtained experimentally by EDX studies.

It is determined that there are 5.25×10^{19} (Mo sites).(g^{-1} support):

For 1ML MoO_3/Fe_2O_3;

No. Surface atoms in Fe_2O_3= 10^{19} m^{-2} (surface approximation for complete coverage of a surface)

For 1ML coverage of MoO_3, the number of Mo sites at this surface will be ¼ x 10^{19} m^{-2}

= 2.5 x 10^{18} m^{-2}

Since surface area of Fe_2O_3= 21m^2g^{-1}, No. Mo sites = 21 x 2.5 x 10^{18} m^{-2}

=5.25 x 10^{19} m^{-2} (Mo sites).(g^{-1} support)

Thus, on 0.5 g of support (which is made experimentally), there are:

5.25 x 10^{19} m^{-2} (Mo sites).(g^{-1} support) × 0.5 g = 2.625×10^{19} Mo sites

In moles, this is:

$$\frac{2.625 \times 10^{19}\text{Mo sites}}{6.02 \times 10^{23}\ \text{mol}^{-1}} = 4.375 \times 10^{-5}\ \text{mol Mo}$$

and in grams:

$$4.375 \times 10^{-5}\ \text{mol Mo} \times 95.95\ \text{g mol}^{-1} = 4.2 \times 10^{-3}\ \text{g Mo}$$

The mass of oxygen in the molybdate monolayer can be determined in an analogous fashion:

10^{19} (O sites).(m^{-2} support) × 21 m^2 g^{-1} x 3/4 = 1.575×10^{20} (O sites) (g^{-1} support)

1.575×10^{20} (O sites) (g^{-1} support) × (0.5 g support) = 7.875×10^{19} O sites

$$\frac{7.875 \times 10^{19}\ \text{O sites}}{6.02 \times 10^{23}\ \text{mol}^{-1}} = 1.3125 \times 10^{-4}\ \text{mol O}$$

1.3125×10^{-4} mol O × 16.00 g mol^{-1} =2.1×10^{-3} g O

The total mass of catalyst, including support is:

[4.2×10^{-3} g Mo] + [2.1×10^{-3} g O] + [0.5 g support] =0.506 g

The weight percent Mo is therefore:

$$\frac{4.2 \times 10^{-3}\ \text{g Mo}}{0.506\ \text{g}} \times 100\% = 0.83\ \text{wt.\% Mo}$$

Pre-reduction analysis:

SEM EDX:

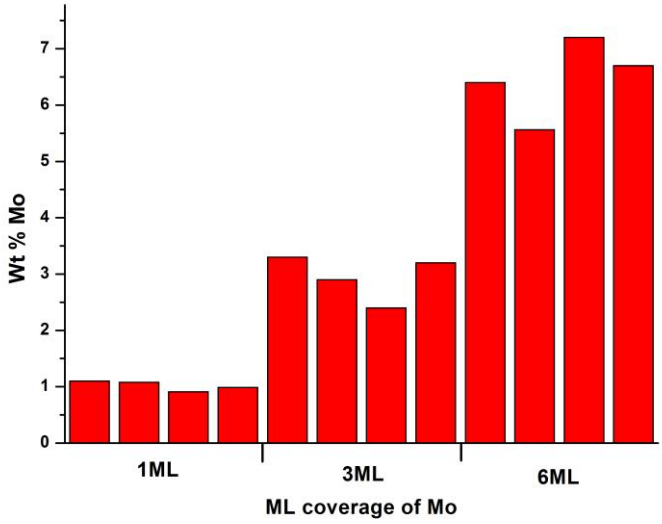

Figure S1. SEM EDX mapping across several areas for 1, 3 and 6ML MoO_x/Fe_2O_3.

TEM EDX:

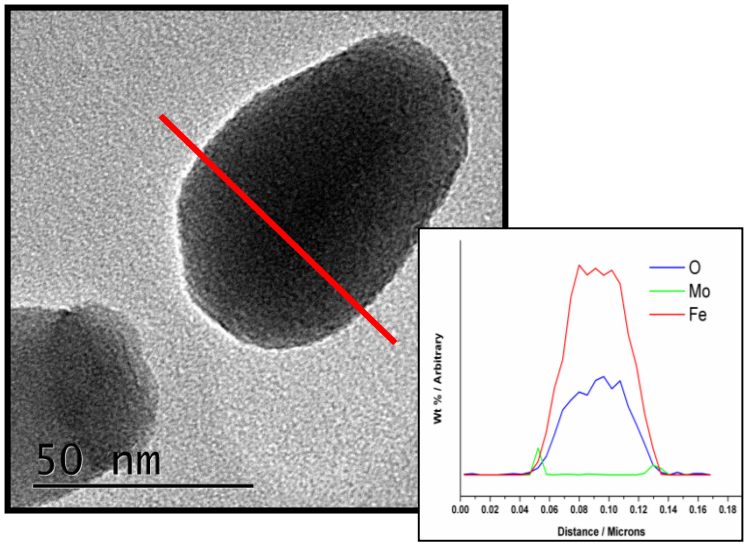

Figure S2. TEM and accompanying EDX line scan data for 1ML MoO_x/Fe_2O_3.

Raman:

Table S1. Raman vibrational bands and their proposed assignments for MoO_3 and $Fe_2(MoO_4)_3$ systems.

Wavenumber / cm^{-1}	**Band Assignment**
667	O-Mo-O symmetric stretch in MoO_3 [1, 2]
700-850	Antisymmetric Mo-O-Mo stretching vibrations in MoO_3[3] Td Mo species in $Fe_2(MoO_4)_3$[4]
780	Mo-O-Mo asymmetric vibrations in $Fe_2(MoO_4)_3$ [5]
816	Mo-O-Mo vibrations in MoO_3[3]
966	Debate in assignments: Mo=O symmetric stretch of the three distinct isolated sites in $Fe_2(MoO_4)_3$[3] Fe-O-Mo asymmetric stretch in $Fe_2(MoO_4)_3$
992	Terminal Mo=O symmetric stretch in MoO_3 [1, 2, 6]

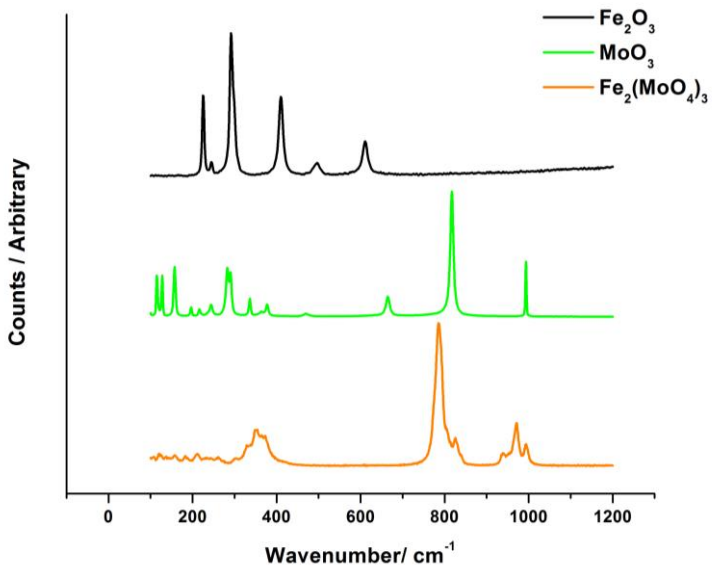

Figure S3. Reference Raman spectra for Fe_2O_3, MoO_3 and $Fe_2(MoO_4)_3$.

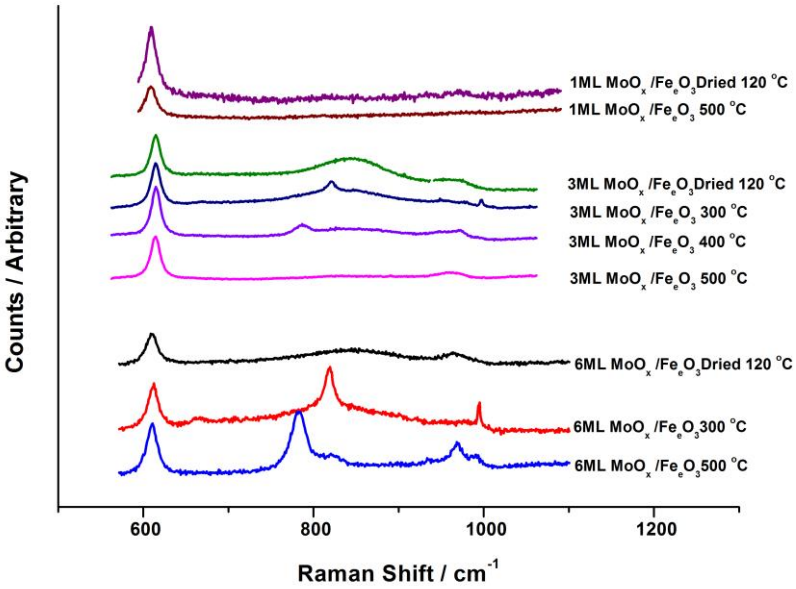

Figure S4. Raman Spectroscopy for 1, 3 and 6ML MoO_x/Fe_2O_3, at varying calcination temperatures, 24 hour calcinations.

XAFS:

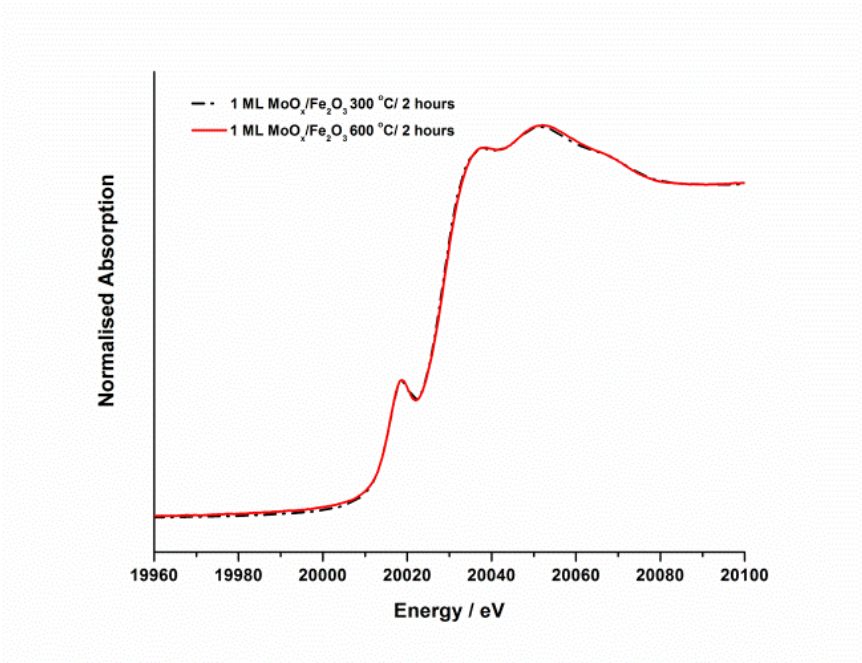

Figure S5. Normalised XANES spectra of 1ML MoO_3/Fe_2O_3 catalysts annealed to 300 and 600 °C, 24 hour calcination.

DRIFTS:

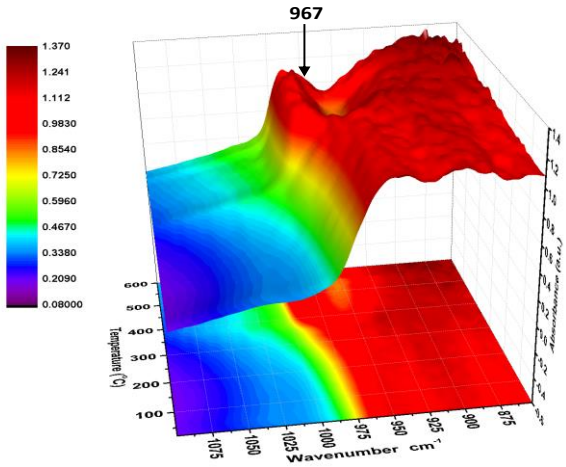

Figure S6. *In situ* DRIFTS spectra of the 6ML MoO_x/Fe_2O_3 during calcination.

DRIFTS spectra (Figure S6) were collected every 15 °C during a 10 °C min^{-1} ramp from room temperature to 600 °C. At approximately 380 °C on both catalysts, a band at 997 cm^{-1} appeared which can be assigned to the Mo=O band of MoO_3. By 560 °C, a band at 967 cm^{-1} appeared consistent with the Fe-O-Mo band of $Fe_2(MoO_4)_3$. [8, 9] These assignments are in agreement with the *in situ* Raman data, which also showed the formation of MoO_3, followed by the formation of $Fe_2(MoO_4)_3$.

Reduction studies:

DR UV/ Vis spectroscopy:

UV/ Vis DRS were collected using a UV-Vis 2600 spectrometer with an integrating sphere. Typically, a portion of the sample was placed into the sample holder and introduced to the integrated sphere. The R % was recorded in the range of 200 – 800 nm, and converted to absorbance using the Kubelka-Munk function. Prior to taking measurements, the baseline was corrected by using $BaSO_4$ as standard. For the reduced samples, a portion of the calcined sample was placed and heated in tube furnace under H_2 at 400 ° C for 2 h, then cooled down to RT in the same atmosphere. The tube containing the sample was sealed well, and transferred into a glove box for the preparation purpose (placed in a homemade PTFE sample holder, covered by a quartz window) prior to each measurement.

The speciation of Mo and Fe ions present in MoO_x/Fe_2O_3 system have been investigated by DR UV/ Vis spectroscopy, after treatment under different conditions. For comparison purposes, the spectra of bulk Fe_2O_3 and MoO_3 materials have also been recorded, with results presented in Figure S7a. It should be noted here, that as there are absorption bands of Mo and Fe based materials in the region of 200 – 400 nm, any absorption bands located in this region should be correlated to both Mo and Fe species. The components located at ~ 220 and 335 nm for MoO_3 bulk phase (Figure S7a, red curve), are due to the charge transfer transitions from *p* oxygen orbitals to *d* molybdenum orbitals ($O^{2-} \rightarrow Mo^{6+}$) of Mo(VI) ions in octahedral structures.[10] The absorption bands observed for Fe_2O_3 bulk material (Figure S7a, black curve) in the range of 300 – 700 nm are in general for the d-d transitions of Fe(III) ions in octahedral structures.[11] Any bands below 300 nm could be ascribed to the charge transfer (CT) of O^{2-} to d Fe orbitals.

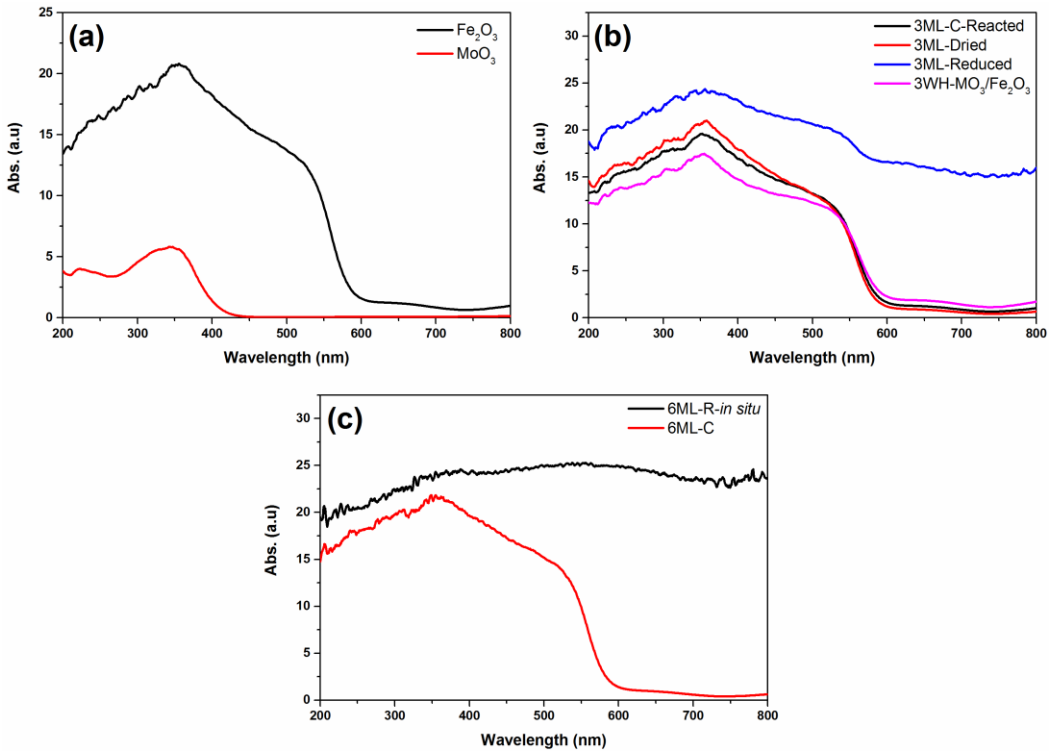

Figure S7. DR UV-Vis spectra of (a) Fe_2O_3 and MoO_3 phases, (b) 3ML MoO_x/Fe_2O_3 at different conditions and (c) 6ML MoO_x/Fe_2O_3 at different conditions. Where, C= Calcined, R= Reduced.

Raman:

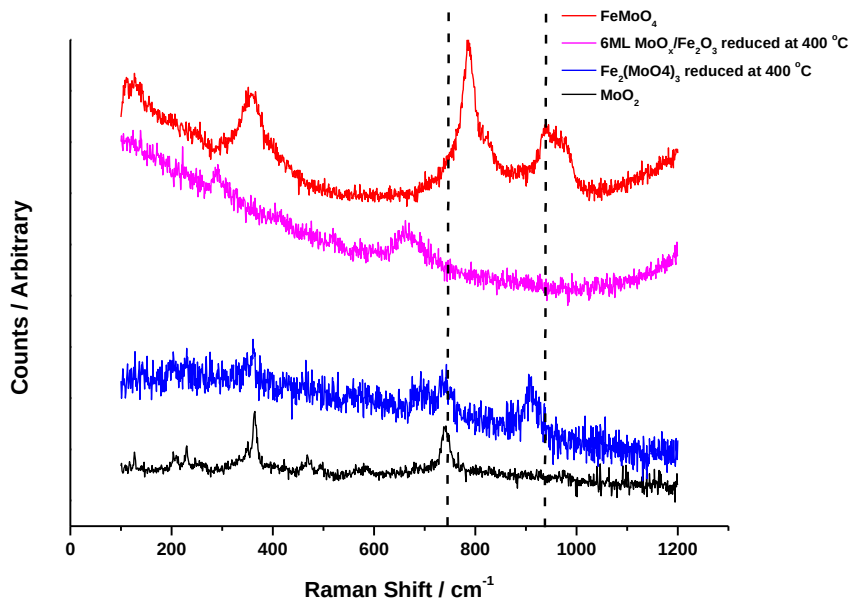

Figure S8. Raman spectra for bulk $Fe_2(MoO_4)_3$ with Mo:Fe ratio 1.7:1, and 6ML MoO_x/Fe_2O_3 after reduction treatment. It is shown that MoO_2 phase formation occurs for the bulk catalyst, but does not for 6ML $MoO_xFe_2O_3$.

XRD:

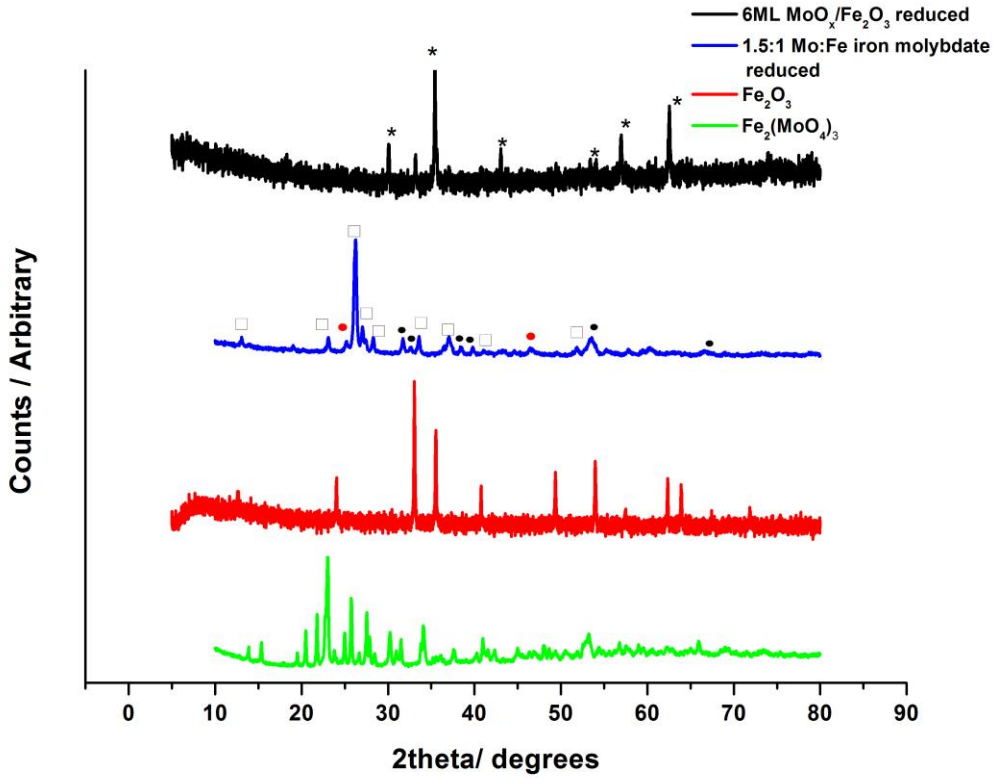

Figure S9. XRD data pre and post-reduction for bulk $Fe_2(MoO_4)_3$, 6ML MoO_x/Fe_2O_3 and references Fe_2O_3 and $Fe_2(MoO_4)_3$. Phases indicated[12]: MoO_2 (black circles), β- $FeMoO_4$ (white squares), and Fe_3O_4 (asterix).The results agree with the findings of the Raman.

XRD was performed using a Panalytical X'pert pro analyser with Cu K- alpha radiation across a 2θ range of 0-80 ˚. Data corroborates that seen through vibrational spectroscopy; for iron molybdate with a Mo:Fe ratio of 1.7:1, the catalyst is composed of MoO_2 shown through the bands at 26, 38 and 53 ˚ 2θ, corresponding to the (011), (020) and (022) reflections.[13, 14] In addition to this, there is strong evidence for β- $FeMoO_4$, most easily identified through the Bragg peaks at 12.97˚ and 26.31˚ 2θ. This extends upon the information obtained through Raman. In contrast, for the 6ML $MoOx/Fe_2O_3$ catalyst, these phases were not observed, showing reduced Fe_2O_3 in the form of Fe_3O_4.[15] Peaks at 30.08, 35.35, 43.06, 53.41, 57.09, and 62.62˚ 2θ, correspond to the (220), (311), (400), (422), (511) and (440) planes respectively.

EXAFS:

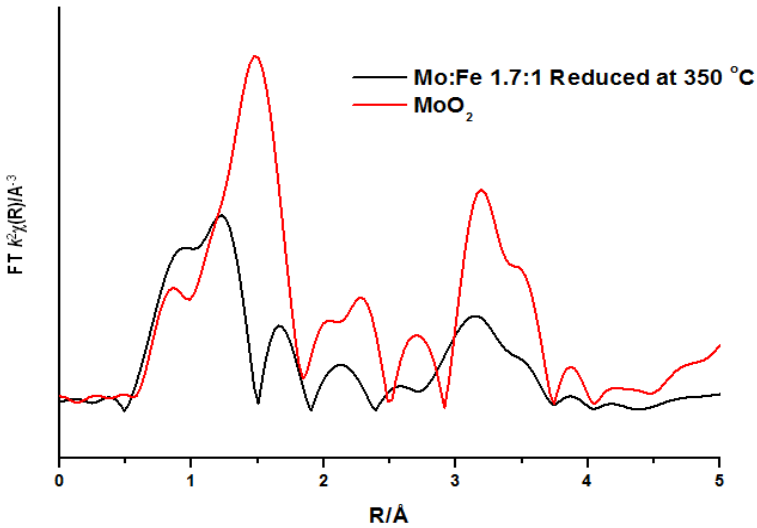

Figure S10. k^2 weighted Fourier Transform data for MoO_2 and bulk Mo:Fe 1.7:1, reduced at 350° C *ex situ*. For bulk $Fe_2(MoO_4)_3$ after reduction *ex situ*, the primary Mo environment is comprised of oxygen neighbours, attributed to the Mo-O bonds in the reduced forms of the molybdenum compounds. These are associated with a shorter Mo^{4+}–O distance found in MoO_2 , and a longer Mo^{6+}-O distance, accredited to $FeMoO_4$, a known reduced form of $Fe_2(MoO_4)_3$. Additionally, further out in R-space, there is a significant shell at 2.5 Å representing a Mo^{4+}- Mo^{4+} interaction [56]. This is analogous to the bonded Mo-Mo unit found within the di-nuclear units of MoO_2.There is a consistent match in term of phasing and amplitude between the materials, especially at further out values of *k*. Data agrees well with that seen through Raman and XRD, confirming the production of MoO_2 in this bulk catalyst.

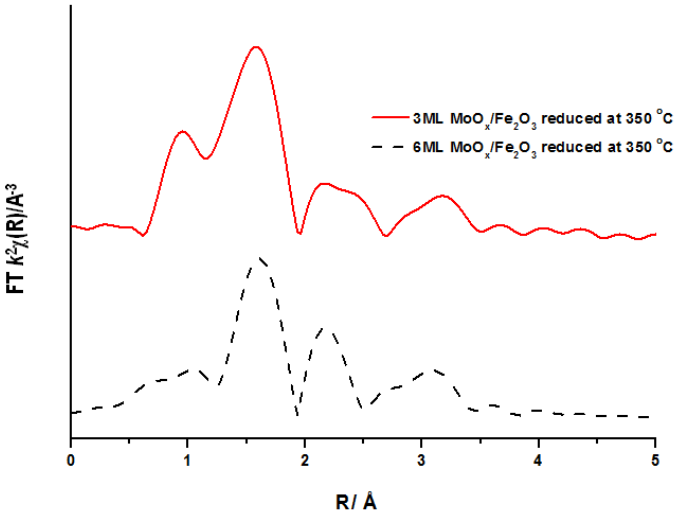

Figure S11. k^2 weighted Fourier Transform data for 3 and 6ML MoO_x/Fe_2O_3 reduced at 350 °C.

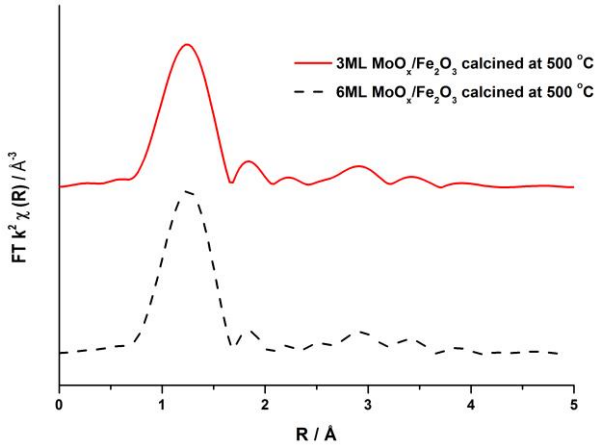

Figure S12. k^2 weighted Fourier Transform data for 3 and 6ML MoO_x/Fe_2O_3 calcined at 500 °C

Table S2. Selected bond distances for MoO_3 and $Fe_2(MoO_4)_3$. [16-19]

Catalyst	Bond Distance / Å	Assignment
MoO_3	1.67	Mo-O(1)
	1.73	Mo-O(2)
	1.94	Mo-O(3)
	2.25	Mo-O(2)′
	2.33	Mo-O(3)′
$Fe_2(MoO_4)_3$	1.987	Fe(1)-O(1)
	1.973	Fe(1)-O(2)
	1.978	Fe(1)-O(3)
	1.969	Fe(1)-O(4)
	2.005	Fe(1)-O(5)
	1.989	Fe(1)-O(6)
	1.746	Mo(1)-O(2) x 2
	1.733	Mo(1)-O(4) x 2
	1.757	Mo(2)-O(1)
	1.737	Mo(2)-O(3)
	1.736	Mo(2)-O(5)
	1.725	Mo(2)-O(6)

BET:

Table S3. Surface areas for various catalysts pre and post reduction.

Sample calcined at 500 ° C	**Surface Area / m^2g^{-1}**
Commercial Fe_2O_3 (<50nm)	21
1ML MoO_3 /Fe_2O_3 pre- reduction	20
3ML MoO_3 /Fe_2O_3 pre- reduction	15
6ML MoO_3 /Fe_2O_3 pre- reduction	12
3ML MoO_3 /Fe_2O_3 dried 120 ° C	16
3ML MoO_3 /Fe_2O_3 calcined at 300 ° C	15

3ML MoO_3 /Fe_2O_3 calcined at 400 ° C	14
3ML MoO_3 /Fe_2O_3 calcined at ° C	15
$Fe_2(MoO_4)_3$	4.5
MoO_3	0.6
Fe_2O_3 reduced at 350 °C in MeOH/He	21
1ML MoO_3 /Fe_2O_3 reduced at 350 °C in MeOH/He	17
3ML MoO_3 /Fe_2O_3 reduced at 350 °C in MeOH/He	14
3ML MoO_3 /Fe_2O_3 reduced at 350 °C in MeOH/He	11

Catalytic testing

Catalytic testing of the reduced samples (Figures 13- 15) was performed using TPD of MeOH/He. Desorption profiles for reduced 1 and 6ML MoO_x/Fe_2O_3 and reduced iron molybdate are presented.Referring to the different catalysts, all produce CO, H_2CO, H_2 and CO_2 during the desorption process. Water is also seen for all profiles, with two peaks occurring. The first is coincident with methanol since the solution used is an aqueous solution, and the second, at a higher desorption temperature coincident with CO_2 as a combustion product **(Equation 1).**

$$CH_3OH\ (g) + 3O_a \rightarrow HCOO_a + H_2O\ (g) + OH_a \rightarrow CO_2\ (g) + 2H_2O\ (g) \qquad \textbf{Equation 1}$$

The CO by-product is consistent with isolated Fe sites, where a change in binding energy at Fe-O-Mo bridging oxygen encourages dehydrogenation of the adsorbed methoxy intermediate.

The higher temperature H_2 and simultaneous CO_2 production is consistent with methanol decomposition *via* formate intermediate (**Equation 1**), which is also indicative of the presence of more Fe at the surface after this reduction procedure, especially the presence of dual sites of iron. Clearly there is a higher population of these for the 1 ML catalyst compared with the 6ML sample.

Disregarding the differences in the onset temperature of the various by- products, on assessment of these data, there appears to be a strong correspondence between the reduced bulk and monolayer catalyst reactivity profiles, with all producing H_2 and CO_2 as the major products. Since monolayer and bulk reduced catalysts perform so similarly, this would infer a similar surface termination in each of these materials. Information obtained from catalytic testing implies that we have aggregated clusters of Mo after reduction, with the majority of the surface comprised of exposed Fe_3O_4. The presence of this Fe rich phase leads to the adsorption of bidentate formate, responsible for the rises in CO_2 and H_2, and ultimately for poor selectivity to formaldehyde.

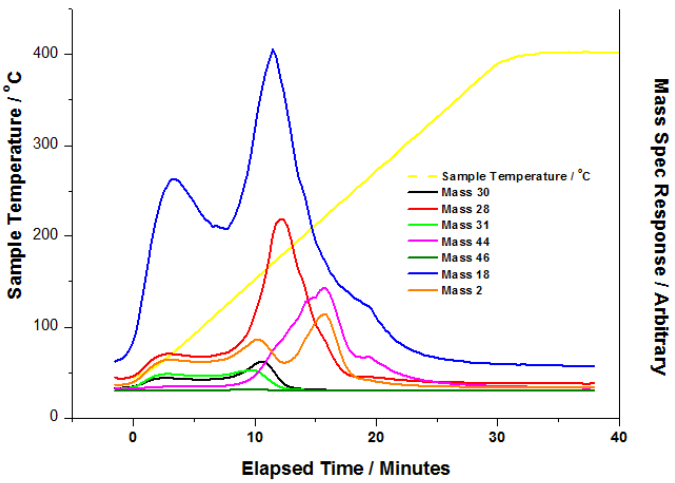

Figure S13. TPD of MeOH/He for 1ML MoO_x/Fe_2O_3 after reduction at 350 °C.

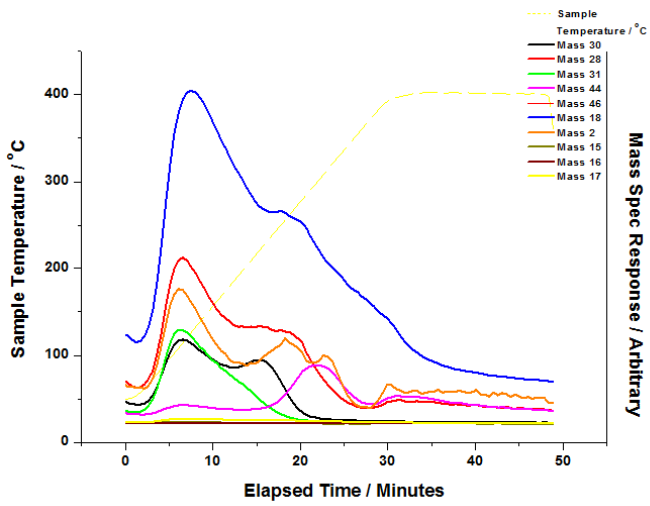

Figure S14. TPD of MeOH/He for 6ML MoO_x/Fe_2O_3 after reduction at 350 °C.

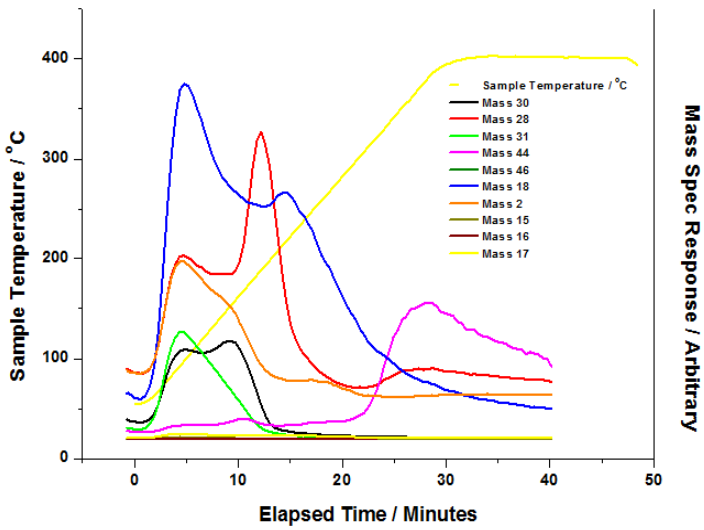

Figure S15. TPD of MeOH/He for Bulk $Fe_2(MoO_4)_3$ after reduction at 350 °C. Less CO_2 at 260 °C, since more lattice oxygen available to the surface.

References

1. K. Routray, W. Zhou, C. J. Kiely, W. Grünert and I. E. Wachs, *J. Catal.*, 2010, 275, 84-98.
2. L. E. Briand, A. M. Hirt and I. E. Wachs, *J. Catal.*, 2001, 202, 268-278.
3. K. Routray, W. Zhou, C. J. Kiely, W. Grunert and I. E. Wachs, *J. Catal.*, 2010, 275, 84-98.
4. R. Davies, D. Edwards, J. GrÃ¤fe, L. Gilbert, P. Davies, G. Hutchings and M. Bowker, *Surf. Sci.*, 605, 1754-1762.
5. A. M. Beale, S. D. M. Jacques, E. Sacaliuc-Parvalescu, M. G. O'Brien, P. Barnes and B. M. Weckhuysen, *Appl. Cat. A-Gen.*, 2009, 363, 143-152.
6. H. J. Tian, C. A. Roberts and I. E. Wachs, *J. Phys. Chem. C*, 2010, 114, 14110-14120.
7. G. Ramis, L. Yi, G. Busca, M. d. Arco, C. Martin, V. Rives and V. S. Escribano, *Mater. Chem. Phys.*, 1998, 55, 15.
8. A. A. Belhekar, S. Ayyappan and A. V. Ramaswamy, *J. Chem.Tech. Bio.*, 1994, 59, 8.
9. F. Trifiro, V. D. Vecchi and I. Pasquon, *J. Catal.*, 1969, 15, 9.
10. V. S. Escribano, J. G. Amores, E. F. López, C. del Hoyo Martínez, G. Busca and C. Resini, *Mater. Chem. and Phys.*, 2009, 114, 848-853.
11. A. Jitianu, M. Crisan, A. Meghea, I. Rau and M. Zaharescu, *J. Mater. Chem.*, 2002, 12, 1401-1407.
12. K. I. Ivanov and D. Y. Dimitrov, *Catal. Today*, 2010, 154, 250-255.

13. L. Kumari, Y.-R. Ma, C.-C. Tsai, Y.-W. Lin, S. Y. Wu, K.-W. Cheng and Y. Liou, *Nanotechnology*, 2007, 18, 115717.
14. Z. Xiang, Q. Zhang, Z. Zhang, X. Xu and Q. Wang, *Ceram. Int.*, 2015, 41, 977-981.
15. M. Martín, P. Salazar, R. Villalonga, S. Campuzano, J. M. Pingarrón and J. L. González-Mora, *J. Mater. Chem. B*, 2014, 2, 739-746.
16. J. Volta and J. Tatibouet, *J. Catal.*, 1985, 93, 467-470.
17. M. H. Rapposch, J. B. Anderson and E. Kostiner, *Inorg. Chem.*, 1980, 19, 3531-3539.
18. V. Massarotti, G. Flor and A. Marini, *J.Appl. Crystallogr.*, 1981, 14, 64-65.
19. W. T. A. Harrison, *Mater. Res. Bull.*, 1995, 30, 1325-1331.